Phase-dependent premelting of self-assembled phosphonic acid multilayers

M. de Pauli, R. Magalhães-Paniago, and A. Malachias*
Departamento de Física, Universidade Federal de Minas Gerais, Avenida Antonio Carlos 6627, Belo Horizonte—MG, CEP: 30123-970, Brazil

(Received 20 February 2013; revised manuscript received 10 April 2013; published 13 May 2013)

Melting and premelting phenomena in self-organized organic systems have been extensively explored in the literature, exploring distinct behaviors of different molecule lengths and morphologies. Nevertheless, the influence of the supramolecular assembly configuration on the occurrence of premelting remains poorly explored. Here we use phosphonic acids as model systems for self-organized molecular assemblies. These molecules exhibit long-range order on different types of substrates. The balance between chain-to-chain and head-to-head interactions leads to distinct types of stackings. Although their structural configurations are well understood, very little is known about their behavior near the melting transition. We show here that premelting occurs in lamellar structures and that its behavior depends directly on the ordered configuration assumed in the studied multilayers. Two molecules with different chain lengths were investigated: octadecyl phosphonic and octyl phosphonic acids. Although almost no dependence on the molecule length was observed, the occurrence of premelting is strongly influenced by their lamellar packing configuration. For tilted packings premelting is unfavored while in straight configurations, where alkyl chain interactions are weakened with respect to head-to-head interactions, strong premelting is observed. We find that the onset of premelting occurs at the domain boundaries with straight lamellar configurations and the domain sizes exhibit power law temperature dependences.

DOI: 10.1103/PhysRevE.87.052402 PACS number(s): 61.05.cp, 64.75.Yz, 64.70.M−

I. INTRODUCTION

Melting phenomena have historically triggered research interest in different scientific communities [1]. Studies of melting have been performed on bulk, surface, and interface states of inorganic compounds [2–4]. Organic systems were also investigated and reveal that in some particular conditions the sample history, film thickness, and amount of piled layers strongly affect the observed transitions [5–8].

Bulk melting is a typical first order transition, where the transformation from solid to liquid for a fixed pressure occurs at a single temperature. This is due to Gibb's phase rule [9], which states that the number of phases P of a system is equal to the number of components C minus the number of degrees of freedom F plus 2, i.e., $P = C - F + 2$. In the case of a one component system $C = 1$ and therefore $P = 3 - F$. This means that if the system is in a single phase (say, solid) with $P = 1$ only two variables can be varied ($F = 2$, say temperature and pressure). However, if two phases coexist (e.g., solid and liquid) $P = 2$, and therefore $F = 1$, only one degree of freedom (either temperature or pressure) can be varied. In such scenario once pressure is determined these two phases will coexist only for a single temperature.

This phase rule does not forbid, however, the possibility of premelting of the border of phase domains, since if the system is finite surface tension has to be taken into account. Several works have already studied premelting, especially in the very important case of the ice surface [2,4]. It was found that a quasiliquid layer grows following a logarithmic law of the type $d \sim 1/\ln|T - T_c|$ [2,3]. The case of premelting of self-assembled phosphonic acid multilayers, a simplified system that can shed light on the understanding of many other organic compounds, has not yet been addressed.

Phosphonic acids are amphiphilic molecules composed of a phosphonic head and an alkyl chain with a variable number (n) of methyl groups [general formula $CH_3(CH_2)_nPO(OH)_2$]. Due to their self-assembly properties [10] they are suitable molecules for applications such as coatings and surfactants [11–14], monolayers in organic electronics and optical devices [15–18], and adhesives [19]. On the other hand, they are model systems for molecular interactions in fatty acids, and can achieve configurations that range from micelles to functionalized thin films compatible with cellular membranes [20].

In this work we study the premelting of multilayers of phosphonic acids with two distinct chain lengths. It has already been found that the premelting transition behavior for fatty acids is independent of the alkyl chain size [21], while in many other molecules size and morphology rule the overall melting behavior [22,23]. Here we have found that although the alkyl chain size is not crucial for the occurrence of premelting phenomena, distinct packing configurations of these molecules modify the transition behavior, leading to premelting characteristics that can impact the performance of devices based in this class of compounds. In particular, we observe that premelting takes place for phosphonic acids domains of straight aligned bilayers. In the case of tilted stackings, premelting is almost not present. We also find that the lateral correlation length of the domains follows a power law of the type $\xi \sim |T - T_c|^{\varphi}$, in contrast with premelting of bulk materials. We finally observe that the temperature evolution of the lamellar (out-of-plane) lattice parameter depends on the different stackings of these phosphonic acids, i.e., tilted stackings exhibit a continuous lattice parameter expansion, while straight configurations do not show any variation.

II. EXPERIMENT

A. Atomic force microscopy and x-ray measurements

Two phosphonic acids with different chain lengths were investigated—octadecyl phosphonic acid [ODPA,

*angeloms@fisica.ufmg.br

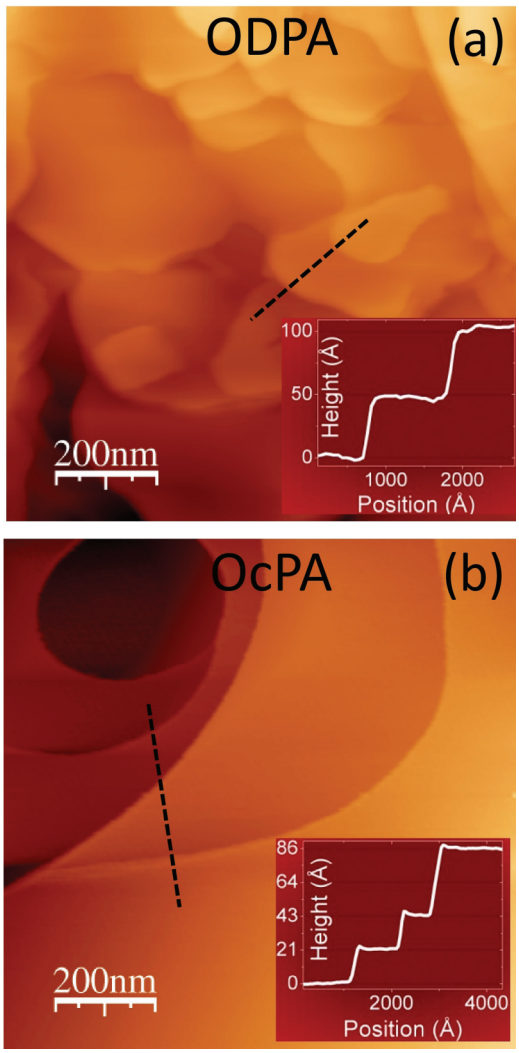

FIG. 1. (Color online) AFM images of (a) ODPA and (b) OcPA multilayers. The insets show the height profiles along the dashed lines of the main figures.

$CH_3(CH_2)_{17}PO(OH)_2$] with molecules with 25 Å length, and octyl phosphonic acid [OcPA, $CH_3(CH_2)_7PO(OH)_2$] which has molecules with 13 Å length. The self-assembly of amphiphilic molecules is related to their polar structure consisting of a hydrophilic head and a hydrophobic tail. The deposition procedure used here (spread coating; see Refs. [10,24,25]) leads to the formation of several stacked ODPA or OcPA bilayers allowing to explore molecule-molecule interactions (bulk state) that are largely independent from the substrate choice. All samples were prepared using a 5 mM concentrated solution of each molecule (ODPA and OcPA) diluted in ethanol. A micrometric pipette was used to spread coat the solution on silicon (100) substrates with native SiO_2 layers (∼25 Å thick, 2 Å rms surface roughness). The solution was deposited in steps of 1 μl. The total amount of solution deposited for ODPA samples was 4 μl and for OcPA was 9 μl. The ethanol solvent was evaporated using a slow flow of ultrapure nitrogen.

Initially, Atomic Force Microscopy (AFM) measurements at room temperature were performed to confirm the existence of ordered bilayer stacks as described in previous works [24,26]. A Veeco Nanoscope IIIa from the MTA group at the Brazilian Synchrotron Light Laboratory (LNLS) was used. In Fig. 1(a) we show an AFM image of ODPA multilayers. The inset depicts a height profile along the dashed line marked in the figure. Such topographic profile shows the presence of 50 Å steps due to ODPA molecule bilayers. The AFM image of OcPA is shown in Fig. 1(b), where the topographic profile (inset) reveals the presence of 21.5 Å steps corresponding to tilted molecule bilayers, forming an angle of 34° with respect to the surface normal [10].

AFM measurements provide information solely on the surface lamellar packing and a more complete probe is required to investigate the system thoroughly. Therefore, x-ray diffraction (XRD) measurements were performed at beamline XRD2 of LNLS using a fixed energy of 8.00 keV [10,24]. In Fig. 2 we show the diffraction data for both phosphonic acids studied here as well as theoretical fits obtained using a kinematical model [27]. The simulated diffraction intensity is obtained as

$$I(q_z) \propto \sum_{n=1}^{N} V_n \left| \sum_{m=1}^{Nl} \sum_{j=1}^{Na} f_j \exp[iq(r_j + md_n)] \right|^2 \times \frac{\exp[-(\sigma q_z)^2]}{q_z^2}, \quad (1)$$

where Na is the number of atoms inside each bilayer, r_j is the position of the jth atom in the bilayer, Nl accounts for the number of bilayers comprising the coherently ordered domain with a given configuration, d_n is the thickness of a bilayer, and σ is the mean interface roughness between the organic bilayers within the structure (acting as a static Debye-Waller attenuation factor). The final intensity in this model is therefore given by the incoherent sum of intensities for a few N coexisting bilayer periodicities, explored in detail in Ref. [10], each with a relative volume fraction V_n (with $\Sigma_n[V_n] = 1$). The parameter f_j is the atomic scattering factor

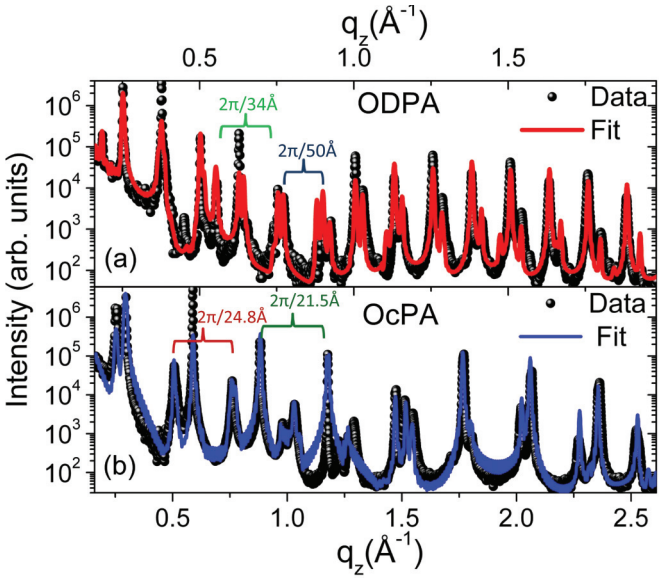

FIG. 2. (Color online) X-ray diffraction measurements (dots) and fits (solid lines) for (a) ODPA and (b) OcPA multilayers.

for the group of atoms in the position j. The number of stacked bilayers [Nl in Eq. (1)] in our phosphonic acid multilayers was found to be of the order of 30 for a large temperature range, thus producing stacks with out-of-plane dimensions ranging from 600 to 1500 Å, depending on the molecule type and packing (out-of-plane projection).

The diffraction data obtained from ODPA multilayers [Fig. 2(a)] at room temperature exhibit different Δq_z intervals between the observed peaks, evidencing the presence of distinct periodicities. The theoretical model reveals the presence of three lamellar periodicities related to different tilt angles of ordered molecules. The periodicity $d1$ represents a straight bilayer configuration with 50 Å. The periodicity $d2$—48.9 Å—is related to tilted bilayer with an angle of 12° with respect to the normal, and $d3$ corresponds to a periodicity of 34 Å (bilayer tilted by 47°). The relative volume fractions of each periodicity were retrieved as $V_1 = 0.890(3)$, $V_2 = 0.050(1)$, and $V_3 = 0.060(1)$. In this work we studied the premelting of the main periodicities of 50 and 34 Å (hereafter referred to as straight and tilted configurations, respectively). The minor phase (V_2) melts at a much lower temperature and seems to be metastable upon deposition.

The XRD data from OcPA multilayers are shown in Fig. 2(b). Again, three distinct periodicities are found. The periodicity $d1$ is related to a straight bilayer packing, 25.9 Å. The configuration $d2$ of periodicity 24.8 Å, is tilted by only 17°, while the configuration $d3$ with 21.5 Å periodicity is tilted by 34°. The relative volume fractions retrieved from OcPA multilayers were $V_1 = 0.008(1)$, $V_2 = 0.062(1)$, and $V_3 = 0.930(3)$. The main periodicities of 24.8 and 21.5 Å were analyzed in this work (they are also mentioned along the text as OcPA straight and tilted configurations, respectively).

The lamellar packing evolution as a function of temperature for ODPA and OcPA multilayers has already been studied [10]. In ODPA samples the tilted configuration (34 Å) is thermally more stable with respect to the straight ordering. On the other hand, in OcPA samples the more stable configurations were found to be those with reduced tilt angle. It is worth mentioning at this point that the thermal evolution of the lamellar packing has not shown any evidence of redistributions between distinct ordered configurations.

B. Transversal scan analysis

In order to determine the correlation length, the interfacial roughness, and the interface roughness exponent—and to infer the occurrence of premelting within the temperature range used for heating the phosphonic acids—the diffuse scattering was analyzed in the vicinity of selected Bragg peaks. Following the formalism of Sinha *et al.* [9] and Geer *et al.* [28,29] the structure factor of the diffuse scattering is given by

$$S(\vec{q}) = \frac{1}{q_z^2} F(q_z) \left[G(q_z) + \sum_{n=1}^{\infty} \frac{(\sigma^2 q_z^2)^n}{n!} \int_{-\infty}^{\infty} e^{-n(|x|/\xi)^{2h}} e^{-iq_x x} \right], \tag{2}$$

where $G(q_z)$ is a narrow Gaussian function centered at the peak position (to take into account the specular reflectivity intensity at q_x values below 0.0003 Å^{-1}), σ is the rms interlayer roughness, ξ is an intralayer correlation length parallel to the surface, and h the interface roughness exponent [28]. Following Sinha *et al.* [9] h provides the fractal dimension D of a surface or interface, given by $D = 3–h$. Therefore values approaching unity are expected for two-dimensional flat interfaces while values approaching zero denote the presence of very rough interfaces.

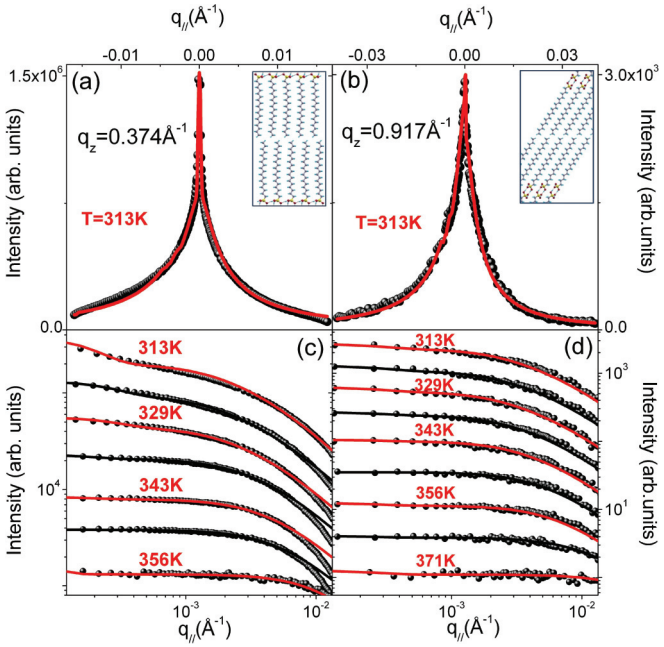

FIG. 3. (Color online) Transversal scans in ODPA multilayers obtained in (a) $q_z = 0.374$ Å^{-1} peak (straight bilayer configuration) and (b) $q_z = 0.374$ Å^{-1} peak (tilted bilayer configuration). The insets of (a), (b) show graphical representations of lamellar order configurations extracted from [10]. (c) and (d) show fits for the peaks depicted in (a) and (b), respectively, for different temperatures in a log-log plot (selected temperatures are indicated). Curves were displaced vertically for better visualization.

In all fittings performed using Eq. (2) the roughness parameter σ was fixed to the value retrieved by the fit of the longitudinal θ–2θ scans (Fig. 2). Therefore, only ξ and h were varied, yielding a reliable procedure for data analysis. Asymmetric profiles were observed experimentally as shown by the dots in Figs. 3(a), 3(b), 4(a), and 4(b). Such effect arises in peaks investigated at low q_z due to changes in the sample illumination under a negative or positive sample angle with respect to the Bragg condition. An illumination correction was included in the model and is observed in the fits that are discussed in the following paragraphs.

The results of single fits for selected peaks at 313 K for Bragg peaks corresponding to straight and tilted bilayer configurations in ODPA multilayers are shown in Figs. 3(a) and 3(b), respectively, with fixed $\sigma = 1.1$ Å. Similar fits at the peaks selected in (a) and (b) were obtained for each investigated temperature (T) and are represented in a log-log plot for selected T's shown in Figs. 3(c) (straight configuration) and 3(d) (tilted configuration), allowing the extraction of both parameters ξ and h. Varying ξ modifies the fit by increasing (decreasing) the intensity difference observed at low (high) $q_\parallel$ values. On the other hand, h values affect mainly the $q_\parallel$ fit

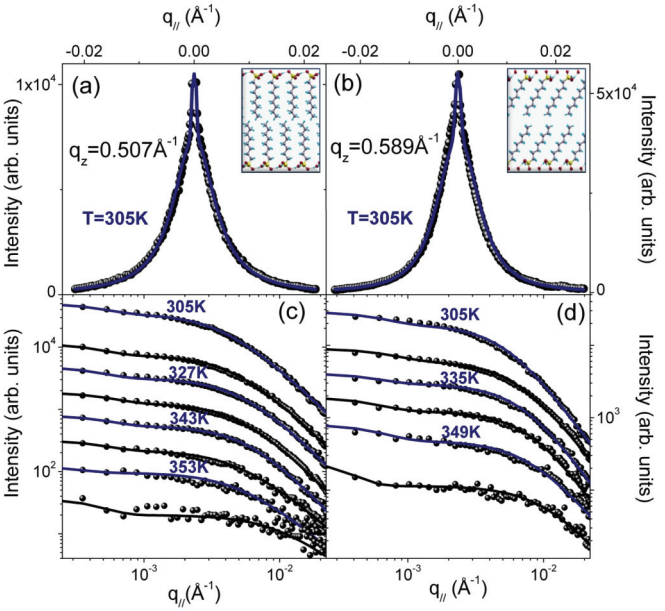

FIG. 4. (Color online) Transversal scans for OcPA multilayers performed in (a) $q_z = 0.507$ Å^{-1} peak (straight bilayer configuration) and (b) $q_z = 0.589$ Å^{-1} peak (tilted bilayer configuration). The insets of (a), (b) show graphical representations of lamellar order configurations extracted from [10]. (c) and (d) show fits in a log-log plot for different temperatures (selected temperatures are indicated). Curves were displaced vertically for better visualization.

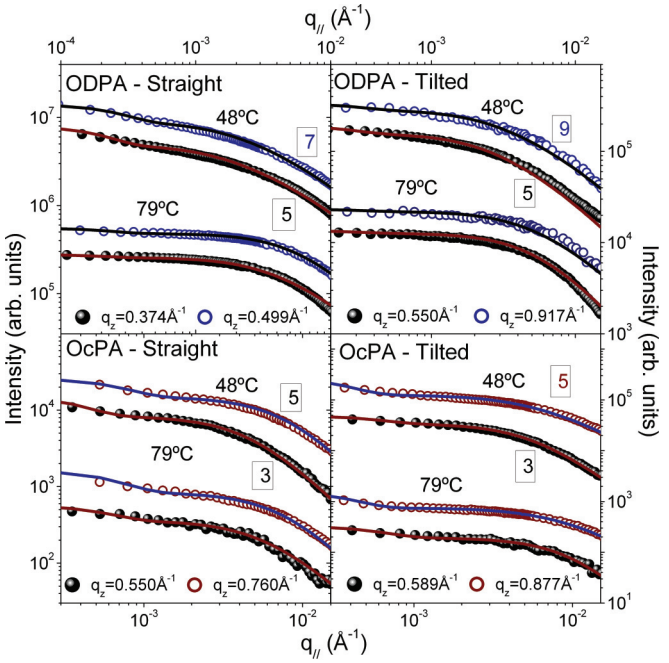

FIG. 5. (Color online) Upper panels: experimental (dots) and fits (solid lines) using Eq. (2) for distinct ODPA multilayer Bragg peaks and different packing configurations at two selected temperatures (48 °C, 79 °C). The left panel refers to straight packing while the right panel refers to tilted packing. For each temperature and packing the parameters ξ and h used to produce the fits are the same, showing that the analysis is independent of the reciprocal space position. Lower panels: similar data and fits for OcPA multilayers.

decay (making it more or less pronounced), providing distinct inflections as one moves further out of the Bragg condition.

Similar results, obtained for OcPA multilayers are shown in Fig. 4. Figure 4(a) shows a $q_\parallel$ scan at $T = 305$ K for a q_z peak position referring to the straight bilayer configuration while Fig. 4(b) shows a similar scan for a peak that arises from the tilted bilayer packing. Fits for selected temperatures, with $\sigma = 1.2$ Å, are shown in Figs. 4(c) and 4(d) for the same reciprocal space positions of (a) and (b), respectively. The behavior of the correlation parameters extracted from the fits of Figs. 3 and 4 will be discussed in the following section.

Distinct packing configurations studied for ODPA and OcPA multilayers exhibit different melting temperatures (premelting behavior is discussed in the following sections). The melting temperature of the ODPA straight configuration [Fig. 3(c)] is $T_c = 356$ K. In the tilted configuration [Fig. 3(d)], thermally more stable, the lamellar order remains up to $T_c = 371$ K. In OcPA multilayers, the straight configuration is more stable [Fig. 4(c)], exhibiting $T_c = 371$ K while the melting temperature for the tilted configuration is $T_c = 357$ K [Fig. 4(d)].

It is known that transversal scan line broadening can vary if the ordered domain sizes are close to the coherence length of the x-ray source. This has been explored for laboratory sources by Stömmer and Pietsch [30], where it is shown that a variation of the linewidth as a function of the reciprocal space peak position is retrieved when the coherent length of the source is proportional to the domain size. In our case, the use of synchrotron radiation with a coherence length much larger than domain sizes and a setup with a high reciprocal space resolution provide experimental conditions that minimize or exclude such possibility.

At this point we have shown only the analysis that allows for extracting the parameters ξ and h from one chosen peak for each phosphonic acid and packing phase type. The question may arise whether the model of Geer *et al.* [28] is valid to properly describe the data sets shown in Figs. 3 and 4 and the robustness of their model. Moreover, the direct evaluation of ξ and h in our model can also be used to rule out the existence of limitations due to the coherence length. In Fig. 5 experimental data retrieved from ODPA and OcPA multilayers at different Bragg conditions for each packing configuration and for two selected temperatures—48 °C and 79 °C—are shown. In all cases the data were fitted with Eq. (2). In the upper panels one sees experimental data (dots) and fits (solid lines) for the diffuse scattering of one lower index straight (tilted) peak and one higher index straight (tilted) peak for ODPA multilayers. For each temperature in the data set the same values of ξ and h are retrieved from the fitting procedure, independently of the superstructure peak order (also shown in the figure). At higher temperatures, as depicted by the selected data in Fig. 5, the behavior of the diffuse scattering changes, requiring distinct parameter values to perform a proper fit. Therefore, although a temperature dependence of ξ and h exists, modifications in the parameter values according to the reciprocal space position were not observed. The lower panels of Fig. 5 exhibit similar data for the OcPA multilayers.

III. RESULTS

In spite of the different alkyl chain lengths the thermal expansion of both acids in the lamellar out-of-plane direction exhibits similar trends. Molecular packings in phosphonic acids can be understood as an energetic competition between hydrogen bonds (HB), present in the phosphonic heads [10] and van der Waals (vdW) interactions between alkyl chains that can lead to an interlock of CH_2 groups (for a thorough discussion see Refs. [10,31]).

Kinematical fits of the longitudinal θ–2θ scans were performed for the temperature series measured for the phosphonic acids in this work. The peak positions retrieved from the complete diffractograms were used to evaluate the evolution of the lamellar thickness (bilayer spacing) as a function of the temperature. Figures 6(a)–6(d) show these results for the straight and tilted configurations in ODPA and OcPA multilayers. The thermal expansion coefficient α for a given bilayer configuration can then be evaluated as $\alpha = \Delta L/(L_0 \Delta T)$, where L_0 is the bilayer thickness at a reference temperature, ΔL the observed thickness variation, and ΔT the temperature interval. In the case of tilted configurations HB and vdW interactions are present and their continuous influence in both molecule multilayers leads to a smooth linear bilayer expansion in the probed temperature range. Although the observed α values are different, they can be better understood taking into account the layer tilt and the projection of the molecule length along the out-of-plane direction. If one considers the ratio between molecule out-of-plane projection and the α values as a renormalized thermal expansion along the molecule longitudinal axis, similar dilations are found for ODPA and OcPA [Figs. 6(b) and 6(d)].

Straight configurations of both acids show a very distinct behavior. A clear thermal expansion is measured up to $T/T_c = 0.88$. For higher temperatures no further change in the bilayer spacing is observed. In these configurations the HB interactions of the heads prevail over the vdW interactions of the alkyl chains.

The observed behavior is then compatible with premelting phenomena as described in Ref. [3]. During this temperature interval changes in the in-plane lattice parameter take place. In the insets of Figs. 6(a) and 6(b) we show the in-plane lattice parameter d for ODPA multilayers obtained by wide-angle x-ray scattering (WAXS) measurements. The continuous increase in lattice parameter as a function of temperature also reinforces the existence of a premelting scenario. The in-plane lattice parameter observed by WAXS in ODPA could not be retrieved in OcPA multilayers where a more disordered in-plane state probably exists [10]. Given the similarities of the two systems, we can assume at this point that premelting occurs in multilayers of both molecule types for straight configurations.

The α coefficients retrieved for straight configurations cannot be quantitatively compared with the figures obtained for tilted configurations since they lie in a small number of points (for the straight OcPA configuration it represents a lower bound). However, one can infer that during the temperature range where expansion is observed, the ratio between the molecule out-of-plane projection and the α value is quite similar for the ODPA tilted and straight packings. This indicates that thermal dilation is mostly independent

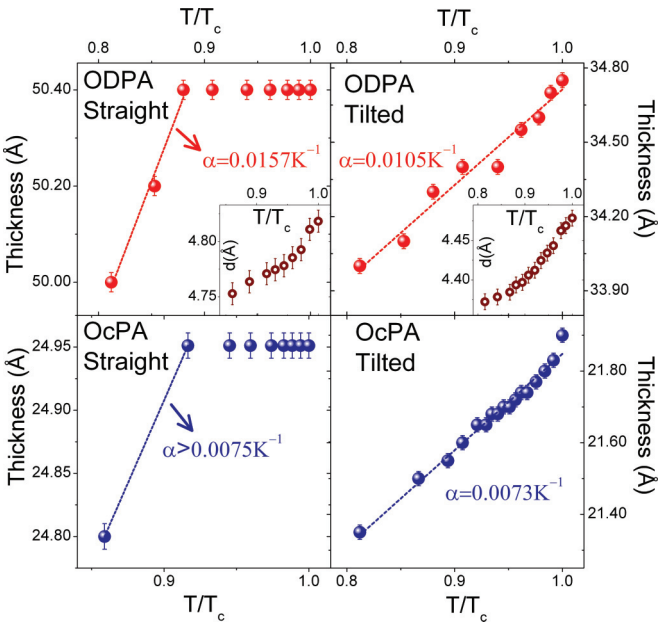

FIG. 6. (Color online) Evolution of lamellar bilayer spacing for ODPA (upper panels) and OcPA (lower panels) configurations as a function of the temperature. The straight configurations exhibit premelting behavior before the melting temperature is achieved. The insets at the upper panels show the temperature evolution of in-plane lattice parameter d from WAXS measurements performed on ODPA multilayers (not shown here).

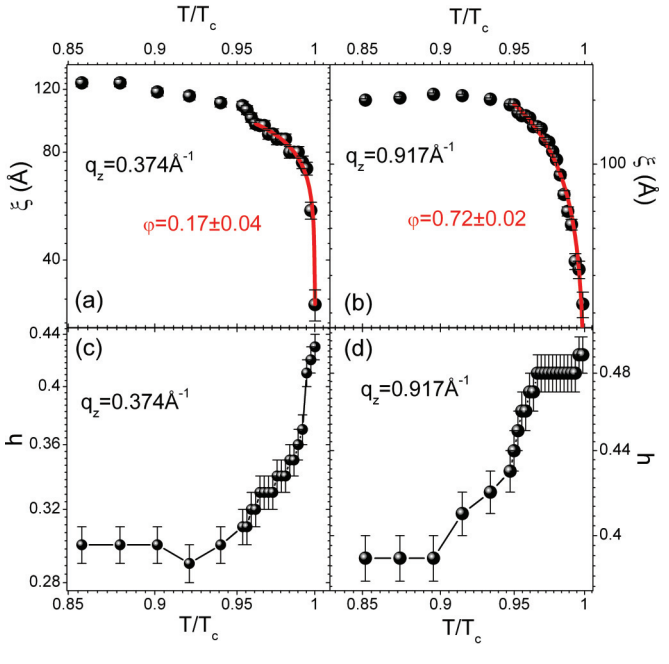

FIG. 7. (Color online) ODPA multilayers: intralayer correlation length as a function of temperature for (a) straight bilayer configuration and (b) tilted bilayer configuration. Solid lines near $T/T_c = 1$ are power law fits of the type $\xi(T) = C_0|T - T_c|^{\varphi}$ (see Discussion section). (c) and (d) show the roughness exponent h as a function of temperature for straight and tilted packings, respectively. In this figure some error bars may be smaller than the symbols.

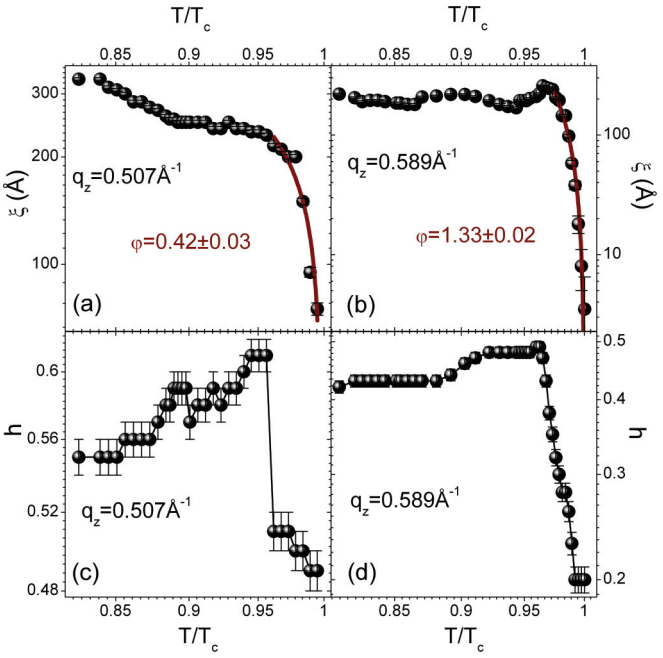

FIG. 8. (Color online) OcPA multilayers: correlation length ξ as a function of temperature for (a) straight bilayer configuration and (b) tilted bilayer configuration. Solid lines near $T/T_c = 1$ are power law fits. (c) and (d) exhibit the correlation decay as a function of temperature. In the figure above some error bars may be smaller than the symbols.

from molecule-molecule interactions and can be mainly ascribed to the linear expansion of individual molecules. The discontinuity of the thermal expansion for straight configurations may lie on the stronger HB interactions (head-to-head) with respect to vdW interactions, indicated by in-plane dilation of the ODPA tilted phase.

The evolution of the parameters ξ and h for ODPA multilayers is shown in Fig. 7, while similar data are extracted for OcPA multilayers in Fig. 8. The general trend of ξ for all molecules and configurations is a nearly constant intralayer correlation length for a broad temperature range followed by a sudden drop near $T/T_c = 0.95$. On the other hand, h values extracted from the fits show a small increase in the roughness exponent for ODPA multilayers for $T/T_c > 0.90$ while a reduction of h values is observed for OcPA as one approaches T_c. This shows that on approaching the melting temperature the surfaces of the ODPA multilayers become smoother, while OcPA surfaces become rougher. This indicates that for OcPA the CH_2 chains can lose registry inside each lamella, still keeping the much stronger molecule head bonds. In the case of ODPA, since the alkyl chains are much longer, tail interactions are mediated through a larger contact area, which stabilizes the in-plane structure.

IV. DISCUSSION

The premelting phenomena exhibit a clear power law behavior of the type $\xi(T) = C_0|T - T_c|^{\varphi}$ close to the melting temperature. In short, the smaller the exponent φ is the larger is the temperature interval where premelting is observed. It is clear that premelting for straight bilayer configurations in both acids is more pronounced than for tilted bilayer phases. This is probably due to the interlock of CH_2 groups present in tilted configurations [31] which provides more stability to the molecular assembly. Therefore, this premelting exponent φ provides a measure of the in-plane interactions within each lamella.

For ODPA samples, correlation lengths ξ of 120 and 200 Å were observed at room temperature in the straight and tilted packing, respectively. The larger domain size obtained for the tilted configuration is in agreement with the enhanced thermal stability of this molecular arrangement as discussed in Ref. [10]. The power law fit of the intralayer correlation of the straight configuration yields an exponent $\varphi = 0.17(4)$ [Fig. 7(a)], much smaller than the exponent for the tilted configuration, $\varphi = 0.72(2)$ [Fig. 7(b)]. However, h values are similar for each configuration both in magnitude and in temperature behavior, varying smoothly between 0.3 and 0.4 at room temperature and between 0.44 and 0.49 near T_c.

The larger values of the exponent φ obtained for OcPA multilayers in Figs. 8(a) and 8(b) denote a more abrupt premelting. These shorter molecules exhibit φ values of 0.42(3) and 1.33(2) for straight and tilted configurations, respectively, larger than their corresponding values found for ODPA multilayers. This behavior can be ascribed to the shorter alkyl chain length and consequently to a relative reduction of vdW interactions (per volume unit) with respect to HBs in the phosphonic heads. The larger domain size at room temperature is also observed here for the most stable OcPA packing of straight bilayers (see Ref. [10]). Contrary to results in ODPA, h values show a small drop in modulus for the straight configuration but a more pronounced variation for the tilted configuration near T_c. This suggests that for the tilted OcPA bilayers the premelting behavior can be mediated by interactions among different lamellas, which is a plausible scenario in shorter molecules (reduced lamellar spacing).

We should also stress that, in contrast with the findings of Bolm *et al.* [32] for stearate multilayers films, no redistribution between different stacking configurations was observed throughout the whole temperature ramp. This shows that the energy barrier between each stable configuration is so pronounced that at temperatures where ordered configurations are destroyed the entropy term prevails over any possibility of establishing other types of stable stacking. Indeed, domain boundaries and sizes can be affected by temperature along the premelting evolution, as observed by the changes in ξ and h. In particular, for the tilted configuration in OcPA molecules the h factor evolves from values that can be ascribed to nearly two-dimensional interfaces ($h \sim 0.5$) to those of three-dimensional behavior ($h \sim 0.2$). Such change in roughness does not result from a modification in the amount of tilted OcPA molecules but is most probably due to the weak interlock of the short alkyl chains, which represents a small energy barrier with respect to head-to-head interactions. These latter are maximized as the interfaces become less defined, increasing the relevance of short-range interaction between molecule heads in neighboring domains (which become smaller for higher temperatures).

A broad premelting scenario observed for the phosphonic acid multilayers studied in this work is described below, and is also depicted in the sketches of Figs. 9(a)–9(c). For low temperatures phosphonic acid molecules are ordered in

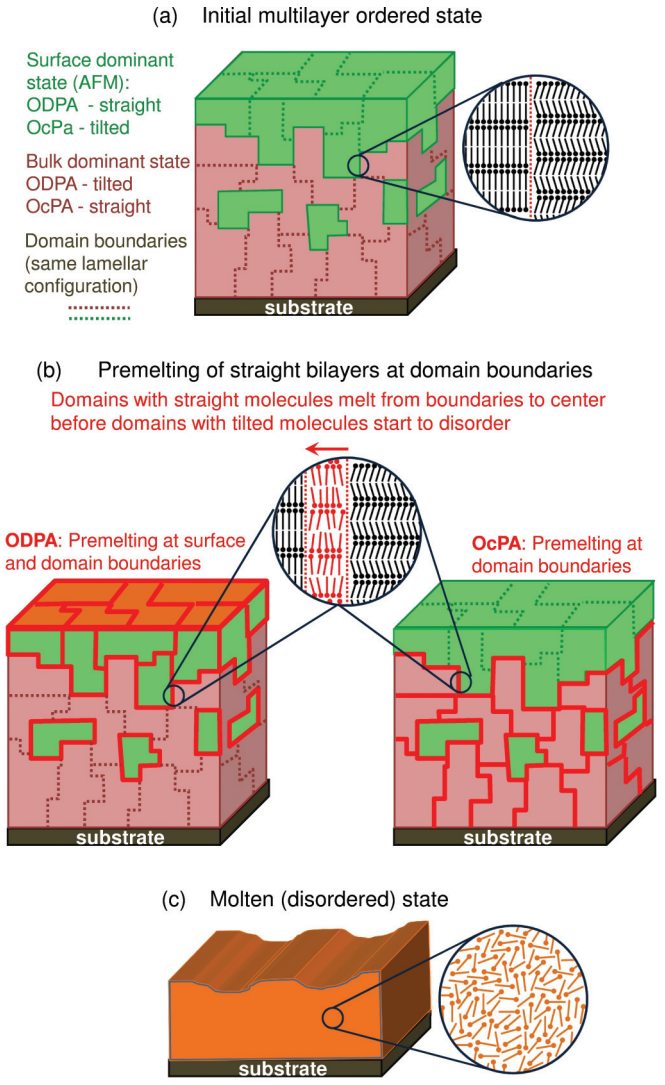

FIG. 9. (Color online) Schematic representations of ODPA and OcPA multilayer melting steps deduced from our work. In (a) domains of ordered molecules coexist at low temperatures. The onset of premelting affects the boundaries of domains with straight molecule packing as shown in (b). These boundaries increase in thickness as the temperature rises, reducing the lateral straight ordered domain sizes before the domains with tilted packing are affected. For temperatures above the melting temperature the system is in a molten state (c).

lamellas composed of bilayers that can stack on straight or tilted phases. While for ODPA the straight phase is observed to be dominant at the sample surface, tilted phases show up at OcPA multilayer surfaces [Figs. 1(a), 1(b); Fig. 9(a)]. Domains of the bulk dominant phase (tilted in ODPA, straight in OcPA) have interfaces with the surface dominant phase (straight in ODPA, tilted in OcPA), given their finite size in the out-of-plane and in-plane directions. Boundaries between domains with the same lamellar configurations may also exist along the in-plane direction, since multilayer scattering produces isotropic (powderlike) intensity rings in WAXS measurements (domain walls are represented by dashed lines in Fig. 9).

As the temperature approaches the melting temperature of the straight phases of both acids—near 0.9 T_c—the in-plane lattice parameter increases while the out-of-plane (lamellar) lattice remains with a constant spacing. Such premelting is also followed by a decrease in lateral domain size ξ in these phases. This is consistent with the onset of a larger disorder in the domain walls of straight configurations, represented by the red molecules in Fig. 9(b). These domain walls become increasingly larger for higher temperatures, providing a one-dimensional boundarylike disorder evolution as also observed by video microscopy in colloidal systems [33]. Finally, as the melting temperature of both tilted and straight phases is achieved, the supramolecular arrangements of both systems pass to the fully disordered state [Fig. 9(c)].

It is clear from Fig. 9(b) that a considerable difference between both systems is the location of the phosphonic acid bilayers with straight configuration. They appear at the surface for ODPA multilayers and in the bulk in OcPA samples. The existence of such straight configurations at the surface implies for the ODPA system that a more effective area for the interfaces that undergo premelting is available. Such scenario is compatible with a reduced φ value with respect to OcPA. As premelting initially takes place for ODPA at the surface state, the roughness exponent h increases with temperature, as a result of the smoothening of the organic/air interface. For the OcPA multilayers the premelting occurs initially at the bulk state. The reduction of h values as the temperature increases reflects an increasing roughness due to the larger bulk disorder among domains.

V. CONCLUSION

Melting behavior is known to depend on the system dimension. In this work we have shown that premelting in phosphonic acids takes place in the boundaries of ordered domains. Although only a weak dependence on the molecule length was observed, the occurrence of such premelting clearly depends on the molecular packing. For straight lamellar stacked molecules the premelting is clearly indicated by the absence of lamellar bilayer periodicity variation in a large temperature interval where the in-plane lattice parameter still changes. This is not observed for tilted molecule stacks, where almost no premelting (or premelting in a very short temperature range) takes place. This behavior can be ascribed to the distinct balance between vdW and HB interactions for each geometry. A power law of the type $\xi(T) = C_0|T - T_c|^{\varphi}$ is found for the domain size dependence on temperature, differently from premelting observed in systems with other dimensions.

The lack of thermal expansion in the straight aligned molecules can be suitable for devices which have monolayers (or few layers) of molecules where the phosphonic acid layer thickness has to be preserved over a working temperature range between 45 °C and 80 °C. This is compatible with the temperature window of current solid state electronic device operation (thus allowing hybrid technology). Knowing if similar premelting behavior can be found in other organic systems of interest has, besides its basic research interest, a potential to open novel organic-inorganic technology integration possibilities for applied research.

ACKNOWLEDGMENTS

The authors thank LNLS (MCT) for experimental support and CAPES for financial support.

[1] J. G. Dash, Rev. Mod. Phys. **71**, 1737 (1999).
[2] A. Lied, H. Dosch, and J. H. Bilgram, Phys. Rev. Lett. **72**, 3554 (1994).
[3] A. Rühm, H. Reichert, W. Donner, H. Dosch, C. Grutter, and J. Bilgram, Phys. Rev. B **68**, 224110 (2003).
[4] S. Engemann, H. Reichert, H. Dosch, J. Bilgram, V. Honkimäki, and A. Snigirev, Phys. Rev. Lett. **92**, 205701 (2004).
[5] M. P. Fontana and P. Facci, J. Chem. Phys. **111**, 5562 (1999).
[6] M. K. Mukhopadhyay, M. K. Sanyal, A. Datta, M. Mukherjee, Th. Geue, J. Grenzer, and U. Pietsch, Phys. Rev. B **70**, 245408 (2004).
[7] D. E. Angelescu, C. K. Harrison, M. L. Trawick, R. A. Register, and P. M. Chaikin, Phys. Rev. Lett. **95**, 025702 (2005).
[8] A. Wildes, N. Theodorakopoulos, J. Valle-Orero, S. Cuesta-López, J. L. Garden, and M. Peyrard, Phys. Rev. E **83**, 061923 (2011).
[9] S. K. Sinha, E. B. Sirota, S. Garoff, and H. B. Stanley, Phys. Rev. B **38**, 2297 (1988).
[10] M. de Pauli, M. C. Prado, M. J. S. Matos, G. N. Fontes, C. A. Perez, M. S. C. Mazzoni, B. R. A. Neves, and A. Malachias, Langmuir **28**, 15124 (2012).
[11] C. A. Barrett, C. Dickinson, S. Ahmed, T. Hantschel, K. Arstila, and K. M. Ryan, Nanotechnology **20**, 275605 (2009).
[12] G. Kopnov, V. Y. Umansky, H. Cohen, D. Shahar, and R. Naaman, Phys. Rev. B **81**, 045316 (2010).
[13] R. Su, H. Liu, T. Kong, Q. Song, N. Li, G. Jin, and G. Cheng, Langmuir **27**, 13220 (2011).
[14] R. Gomes, A. Hassinen, A. Szczygiel, Q. Zhao, A. Vantomme, J. C. Martins, and Z. Hens, Phys. Chem. Lett. **2**, 145 (2011).
[15] H. Klauk, Chem. Soc. Rev. **39**, 2643 (2010).
[16] K. Fukuda, T. Hamamoto, T. Yokota, T. Sekitani, U. Zschieschang, H. Klauk, and T. Someya, Appl. Phys. Lett. **95**, 203301 (2009).
[17] A. Sharma, B. Kippelen, P. J. Hotchkiss, and S. R. Marder, Appl. Phys. Lett. **93**, 163308 (2008).
[18] J. A. Bardecker, H. Ma, T. Kim, F. Huang, M. S. Liu, Y.-J. Cheng, G. Ting, and A. K.-Y. Jen, Adv. Funct. Mater. **18**, 3964 (2008).
[19] M. Maxisch, P. Thissen, M. Giza, and G. Grundmeier, Langmuir **27**, 6042 (2011).
[20] R. M. Fabre, G. O. Okeyo, and D. R. Talham, Langmuir **28**, 2835 (2012).
[21] S. Barman and S. Vasudevan, J. Phys. Chem. B **110**, 22407 (2006).
[22] N. Maeda, M. M. Kohenen, and H. K. Christenson, Phys. Rev. E **61**, 7239 (2000).
[23] D. Fragiadakis and C. M. Roland, Phys. Rev. E **83**, 031504 (2011).
[24] G. N. Fontes, A. Malachias, R. Magalhães-Paniago, and B. R. A. Neves. Langmuir **19**, 3345 (2003).
[25] H.-Y. Nie, M. J. Walzak, and N. S. McIntyre, Langmuir **18**, 2955 (2002).
[26] H.-Y. Nie, N. S. McIntyre, W. M. Lau, and J. M. Feng, Thin Solid Films **517**, 814 (2008).
[27] J. Als-Nielsen and D. MacMorrow, *Elements of Modern X-ray Physics* (Wiley, Chichester, UK, 2001).
[28] R. E. Geer, R. Shashidhar, A. F. Thibodeaux, and R. S. Duran, Phys. Rev. Lett. **71**, 1391 (1993).
[29] R. Shashidhar and R. E. Geer, Int. J. Eng. Sci. **38**, 1049 (2000).
[30] R. Stömmer and U. Pietsch, J. Phys. D: Appl. Phys. **29**, 3161 (1996).
[31] E. Barrena, S. Kopta, D. F. Ogletree, D. H. Charych, and M. Salmeron, Phys. Rev. Lett. **82**, 2880 (1999).
[32] A. Bolm, U. Englisch, F. Penacorada, M. Gerstenberg, and U. Pietsch, Supramolecular Science **4**, 229 (1997).
[33] Y. Peng, Z.-R. Wang, A. M. Alsayed, A. G. Yodh, and Y. Han, Phys. Rev. E **83**, 011404 (2011).